RSC Advances

ROYAL SOCIETY OF CHEMISTRY

www.rsc.org/advances

Journal Name

ARTICLE

Restraining deactivation of hierarchical zeolite supported NiW catalyst in the HDS of thiophene

Received 00th January 20xx,
Accepted 00th January 20xx

DOI: 10.1039/x0xx00000x

www.rsc.org/

Y. Wang,[ab] C. Lancelot,[b] C. Lamonier,[b] M. Yang,[a] Y. Sun,[a*] J. C. Morin,[b] and A. Rives[b*]

NiW catalysts supported on γ-Al_2O_3 (NiW/Al_2O_3), commercial Beta (NiW/HB) and hierarchical Beta prepared by base-acid treatment (NiW/HB-M) were characterized by X-ray diffraction (XRD), N_2 sorption, Infrared spectroscopy (IR), transmission electron microscopy (TEM) and X-ray photoelectron spectroscopy (XPS). The catalytic performance of these catalysts was evaluated in the hydrodesulfurization (HDS) of thiophene. The results indicated that NiW/HB as well as NiW/HB-M endured important and rapid deactivation showing that the introduction of additional mesopores/macropores in support could not prevent the deactivation tendency. Interestingly, NiW/HB or NiW/HB-M mixed with NiW/Al_2O_3 and the utilization of Na^+-exchanged Beta as support improved remarkably the anti-deactivation ability of the catalysts. As a result, the catalysts NiW/NaB-M (NiW catalyst supported on Na^+-exchanged hierarchical Beta) and NiW/20HB-M (20% NiW/HB-M mixed with 80% NiW/Al_2O_3) gave superior catalytic activity than NiW/Al_2O_3.

1. Introduction

Transition metal Ni(Co)Mo(W) sulfide (TMS) catalysts are important industrial catalysts for hydrodesulfurization (HDS) of transportation fuels in oil refinery. Generally, TMS catalysts need to be supported on a carrier like alumina and the support plays a vital role in determining the catalytic activity and stability[1-3]. It is generally accepted that a support with strong Brönsted acid sites is beneficial for promoting the HDS performance of catalysts[4-9] because it could enhance the adsorption property of sulfur-containing molecules[8] and optimizes the electron property of active phases[9]. Thus, zeolites with such acid sites have been widely investigated as support of HDS catalysts[10]. However, some studies indicated that zeolites supported TMS catalysts exhibited lower catalytic activity than alumina supported TMS catalysts in some HDS reactions[11-16]. One explanation is that active phases located in micropores of zeolites might be difficult to access for the reactants. Additionally, it has been reported that microporous zeolite based TMS catalysts underwent a significant deactivation, which could be stabilized during the first few hours [15,16]. Such an initial deactivation would remarkably decrease the activity of zeolite supported catalysts.

To overcome the drawbacks associated to microporous zeolites, the utilization of hierarchical zeolites as support of TMS catalyst has been considered as the active phases located in mesopores/macropores could be more easily accessible to the reactants and the diffusion ability can also be improved due to the introduction of these additional pores. Indeed, there are some reports about this subject. For examples, Ni(Co)Mo catalyst was supported on hierarchical zeolite L[13, 17], ZSM-5[18], and mordenite[19] for HDS reactions. The results indicated that hierarchical zeolites supported Ni(Co)Mo catalyst exhibited superior catalytic performance than microporous zeolites supported one. This demonstrated that the introduction of additional mesopores/macropores in zeolite supports is helpful for enhancing the HDS catalytic performance in agreement with better accessibility of active phases.

On the other hand, it is well known that conventional zeolites deactivated easily in some acid-catalytic reactions and the introduction of hierarchical pores into zeolites can improve the resistance ability to deactivation[20-22]. One explanation is that external active sites outside micropores were able to perform the catalytic function even after active sites inside micropores were deactivated[21]. Thus, from the viewpoint of deactivation the use of hierarchical zeolites as the support of TMS catalysts might inhibit deactivation of catalysts to some extent. Nevertheless, the study about deactivation situation of hierarchical zeolites supported TMS catalysts in the HDS reactions has not been presented.

In this present work, we prepared hierarchical Beta supported NiW catalyst as a representative of hierarchical zeolites supported TMS catalysts. The deactivation of zeolite based catalysts was investigated in HDS of thiophene. The effects of mechanical mixture of the catalysts with NiW/Al_2O_3 and the use of Na^+ exchanged Beta zeolite as support were also considered to restrain the deactivation.

2. Experimental

[a] School of Chemical Engineering and Technology, Harbin Institute of Technology, Harbin, 150001, China.
[b] Unité de Catalyse et Chimie du Solide, UCCS, UMR CNRS 8181,Université Lille Nord de France, 59655 Villeneuve d'Ascq, France.
Electronic Supplementary Information (ESI) available: [details of any supplementary information available should be included here]. See DOI: 10.1039/x0xx00000x

2.1. Materials

Commercial Beta was purchased to the Catalyst Plant of Nankai University. HNO_3, NaOH, NH_4NO_3, $NaNO_3$ were purchased to Sinopharm Chemical Reagent Co., and thiophene to Sigma-Aldrich and used without further purification.

2.2. Preparation of catalysts

H-form conventional and hierarchical Beta: H-form conventional Beta (HB) was obtained by calcining commercial NH_4^+ form Beta zeolite at 823K for 5 h. H-form hierarchical Beta (HB-M) was prepared according to the literature[23]. The sample HB was treated with a solution of 0.2 M NaOH with a liquid-to-solid ratio of 30 ml/g at 338 K for 0.5 h. Then, the product was filtered, washed with deionized water, dried, ion-exchanged into NH_4-form, and calcined at 823 K for 5 h. It was then treated with a solution of 0.1 M HNO_3 at 338 K for 6 h with a liquid-to-solid ratio of 30 ml/g. The product was ion-exchanged as described above, followed by calcination at 823 K for 3 h to obtain the sample labelled as HB-M.

HB and HB-M supported NiW catalysts: The supported NiW catalysts were prepared by co-impregnation using the incipient wetness technique. Typically, the impregnation solution was obtained by dissolution of nickel nitrate hexahydrate and ammonium metatungstate in water with a W/Ni molar ratio of 2.75 based on our previous study[24-27]. The calculated content of WO_3 in catalyst was 15 wt%. These catalysts were dried at 373 K overnight and then calcined at 773 K for 4 h in air, using a temperature ramp of 2 K/min. The chemical composition of various catalysts was listed in Table 1. The HB and HB-M supported NiW catalysts were labelled as NiW/HB and NiW/HB-M, respectively. For comparison, commercial alumina (BET surface area: 220 m^2/g, external surface area: 218 m^2/g, pore volume measured by water adsorption: 0.6 ml/g) supported NiW catalyst prepared by the same method was named as NiW/Al_2O_3.

Table 1. Chemical composition of various catalysts from ICP-OES FAAS measurements and the acidity of supports at 423 K.

Samples	Si/Al	WO_3 (wt%)	W/Ni	Number of Brönsted acid sites (µmol /g)	Number of accessible Brönsted acid sites (×f µmol/g)
NiW/HB	17	16.6	2.4	269	2.0
NiW/HB-M	15	13.1	2.6	209	9.5

Mixed catalysts: The mixed catalysts were prepared by mechanically mixing x wt% NiW/HB or NiW/HB-M (x = 20, 50, 80) with NiW/Al_2O_3 and were accordingly labelled as NiW/xHB or NiW/xHB-M.

Na^+-exchanged conventional and hierarchical Beta: HB or HB-M was treated with 1 M $NaNO_3$ with a liquid-to-solid ratio of 100 ml/g at room temperature for 2 h. This ion-exchanged process was repeated twice. Then, the product was dried overnight, calcined at 823 K for 5 h and labelled as NaB or NaB-M.

NaB and NaB-M supported NiW catalysts: NaB or NaB-M supported NiW catalysts were prepared according to the above-mentioned method. The obtained catalysts were labelled as NiW/NaB and NiW/NaB-M, respectively.

2.3. Catalyst characterization

Inductively Coupled Plasma-Optical Emission Spectroscopy (ICP-OES) results were determined after acidic digestion of zeolites based catalysts in a mixture of fluorhydric acid (3mL) and nitric acid (5 mL) under closed vessels microwave (600 watts) for a duration of 40 minutes. Acidic mineralisations were then analyzed using ICP-OES for nickel, aluminium and tungsten. Silicon was analyses by Flame Atomic Absorption Spectroscopy (FAAS) in order to avoid spectral interference that could exist in ICP-OES. X-ray powder diffraction (XRD) patterns were recorded using a Siemens D-5000 diffractometer equipped with the Cu Kα radiation (wavelength of λ = 1.5418 Å) and using the two cycle diffractometer equipped by six detectors having Si(111) analyzer crystals and Na-I scintillation counters. Nitrogen sorption isotherms were obtained at 77 K on a Micromeritics TriStar II 3020 Gas Sorption and Porosimetry system. Prior to the experiments, the samples were outgassed at 423 K under vacuum for 3 h. Temperature-programmed desorption of NH_3 (NH_3-TPD) was carried out on a Micromeritics AutoChem II 2920 system equipped with a thermal conductivity detector. The samples were first outgassed under 823 K for 1 h before the measurement. After cooling to 373 K, the samples were saturated in an NH_3 stream (5% in Ar) for 1 h and consequently treated in Ar (30 ml/min) for 2 h for removing physisorbed NH_3. Finally, the TPD profile was determined by increasing temperature from 373 K to 873 K with a heating rate of 5 K/min while recording NH_3 desorption with a thermal conductivity detector. The IR studies of pyridine and pivalonitrile adsorption were carried out to measure the number of acid sites and accessible acid sites, respectively, recorded with a Nicolet Protege System 460 equipped with a DTGS detector. All samples were ground in an agate mortar and were pressed into the form of self-supporting wafers (5 mg/cm^2), then heated at 723 K under high vacuum (10^{-6} mbar) for 2 h and cooled down before probe molecule adsorption. All recorded spectra were recalculated to a normalized wafer of 10 mg. The concentration of Brönsted and Lewis acid sites was determined by quantitative IR studies of probe molecule adsorption experiments. In order to quantify Lewis and Brönsted acid sites, FTIR spectrum of the activated surface was substract from the pivalonitrile and pyridine adsorbed one. For experiments based on pyridine adsorption, the following bands and absorption coefficients were used: Pyridinium (PyH^+) band at 1545 cm^{-1}, εB = 1.23 cm/µmol and pyridine (PyL) 1454 cm^{-1}, εL = 1.73 cm/µmol. The concentration of accessible Brönsted and Lewis acid sites was determined by quantitative IR studies of pivalonitrile adsorption experiments using the following bands and absorption coefficients were used: pivalonitrile (PiH^+) band at 2274 cm^{-1}, εB = 0.11/f cm/µmol and pivalonitrile (PiL) 2302 cm^{-1}, εL = 0.15/f cm/µmol, where f was a constant depending on the IR system. For bands with several contributions spectra were decomposed using Omnic software 8.3. X-ray photoelectron spectroscopy (XPS) was performed on an Axis ultra DLD (Kratos analytical) using a

monochromatic Al Kα X-ray source (hv = 1486.6 eV). The emission voltage and the current of this source were set to 15 kV and 10 mA, respectively. The pressure in the analyzing chamber was maintained at 10^{-9} Pa or lower during analysis, and the size of the analyzed area was 300 × 700 μm^2. After their sulfidation under H_2/H_2S (90/10) for 2 h at 673 K, samples were transferred into the spectrometer chamber using a gloves box in order to avoid any reoxydation. Surveys (0~1300 eV) were recorded at pass energies of 160 eV with a step of 1 eV and high-resolution (W4f, Ni2p, S2p and C 1s zone) spectra were recorded at pass energies of 40 eV with a step of 0.1 eV. Data treatment and peak-fitting procedures were performed using Casa XPS software. Obtained spectra were calibrated in respect of C 1s (C–C bond) at 285 eV. The peaks were decomposed using Gaussian–Lorentzian peak shapes. High resolution transmission electron microscopy (HRTEM) analysis was performed on a TECNAI microscope operating at 200 kV with a LaB_6 crystal. Freshly sulfided samples were ground under an inert atmosphere and dispersed in ethanol. The suspension was collected on carbon films supported on copper grids. For statistical analysis, more than 60 photographs were taken for each sample, which enable us to manually measure more than 600 WS_2 slabs. The statistical analysis was performed by measuring the length and stacking number of the slabs.

2.4. Catalytic tests

The HDS of thiophene was performed in a fixed-bed tubular reactor. The reactor was loaded with 0.2 g of catalyst. Then the catalysts were pre-sulfided at atmospheric pressure at 673 K for 3 h (6 K/min) using a mixture of 10 vol% H_2S in H_2 at a total flow rate of 100 ml/min. The reactions were then carried out at 623 K with 20 ml/min H_2 and 1.4 ml/min thiophene. The reaction samples were withdrawn at regular intervals and analyzed by gas chromatography on an Agilent 6890 GC with an FID detector.

3. Results

3.1. Characterizations

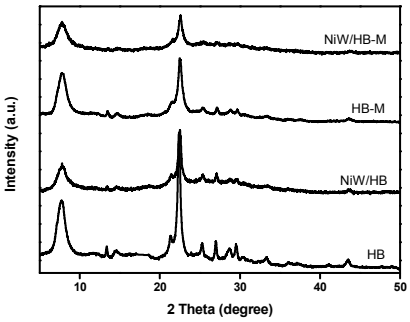

Figure 1. X-ray diffraction patterns of various samples.

The powder XRD patterns of all the samples are presented in Figure 1. HB and HB-M exhibited well resolved diffraction peaks, which are characteristic for beta zeolite framework structure. After supporting NiW catalyst, the zeolite structure was still maintained and no detectable diffraction peaks assigned to WO_3 and NiO were observed. This suggested that tungsten and nickel oxidic species were either completely amorphous or composed of crystallites smaller than 4 nm[28-30], indicating a good dispersion of the metals.

The N_2 sorption isotherms of HB, HB-M and their corresponding catalysts are shown in Figure 2. They exhibited a type I isotherm at low relative pressure and a type IV isotherm with a hysteresis loop at high relative pressure, indicating the existence of hierarchical pores. The detailed sorption data are listed in Table 2. For the catalysts, surface areas and pore volumes were also expressed per gram of support, by deducing the weight gain due to the active phase, in order to estimate the variations of the textural properties of the support itself. It can be observed that the micropore volume, external surface area and mesopore volume of HB and HB-M decreased after impregnation, suggesting that NiW active phase could be dispersed in both micropores and mesopores. The pore distribution of the samples (Figure 2) appeared not affected after impregnation step.

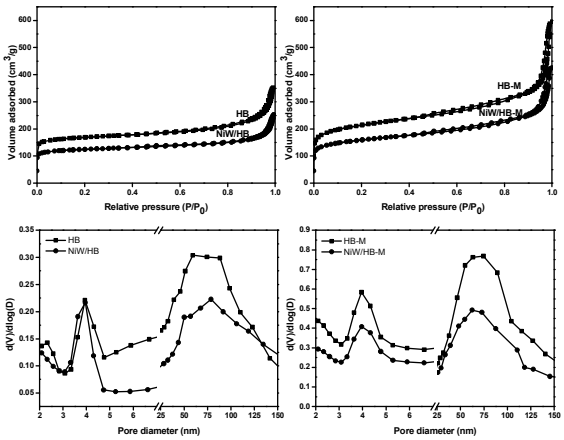

Figure 2. N_2 sorption isotherms and pore distribution of various samples.

Table 2. N_2 sorption data of various catalysts.

Samples	BET surface area (m^2/g)	External surface area (m^2/g)[a]	Micropore volume (cm^3/g)[a]	Mesopore volume (cm^3/g)[b]
HB	550	134	0.20	0.34
NiW/HB	407(507[c])	98(121[c])	0.15(0.18[c])	0.24(0.30[c])
HB-M	717	348	0.18	0.74
NiW/HB-M	531(623[c])	242(284[c])	0.14(0.16[c])	0.52(0.61[c])

a t-plot method.

b BJH method.

c Data calculated by deducting the effect of NiW mass.

The acidity of support was measured by NH_3-TPD and IR study of pyridine/pivalonitrile adsorption to reflect the acidity of catalysts. It can be seen from NH_3-TPD results that both HB and HB-M exhibited two desorption peaks at about 260°C and 450°C (Figure 3), suggesting that they had similar acid strength. The quantity of acid sites is higher in the case of HB support indicating that the treatment of the support led to a decrease of global acidity.

By IR studies of pyridine adsorption (Table 1) it is also shown that HB-M possessed less number of Brönsted acid sites (209 µmol/g) than HB (269 µmol/g) as observed on the global acidity.

In order to try to discriminate between Brönsted acid sites present in micropores and mesopores, a larger basic molecule, pivalonitrile, was used to probe the accessible acid sites. The number of these external Brönsted acid sites is five times larger in HB-M than that in HB in agreement with the larger pore volume of the treated zeolite.

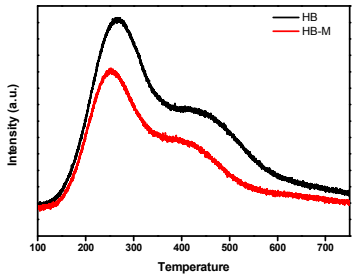

Figure 3. NH_3-TPD profiles for HB and HB-M.

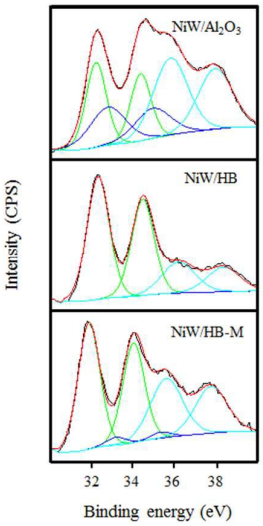

Figure 4. Emission region of W4f XPS spectra of various catalysts sulfided at 673 K with their fit decomposition curves: experimental (black), simulation (red), WS_2 (green), WO_xS_y (blue), W^{6+} (cyan)

Figure 4 showed the XPS spectra of W4f for the sulfided catalysts. The methodology implemented for the decomposition of the spectra of the W4f has been described elsewhere[24-27]. The decomposition of the photopeaks revealed three contributions attributed to W^{6+} in an oxidic environment (W4f5/2: 36.2eV and W4f3/2: 38.3eV), W^{5+} as oxysulfide species (33.2eV and 35.4eV) and W^{4+} sulfided species (32.3eV and 34.4 eV)[25, 27, 31, 32]. The data obtained from these decompositions are listed in Table 3. The WS_2 is representative of the sulfidation degree of tungsten. For NiW/Al_2O_3, it was about 30%, which was in agreement with previous works[27, 33]. In comparison, higher sulfidation degree was obtained for NiW/HB (73%) and NiW/HB-M (58%), which is in accordance with other reported works about that the use of zeolite support improving the sulfidation degree of Ni(Co)Mo(W) catalyst[28, 34]. This result might be related to the relatively weak interaction between active phase and zeolitic support because Si species had weaker interaction than Al species with Mo(W) active phase[35].

Table 3. Percentage of various W species in catalysts after sulfidation.

Samples	WS_2 (%)	WO_xS_y (%)	W^{6+} (%)
NiW/Al_2O_3	30	24	46
NiW/HB	73	0	27
NiW/HB-M	58	3	39

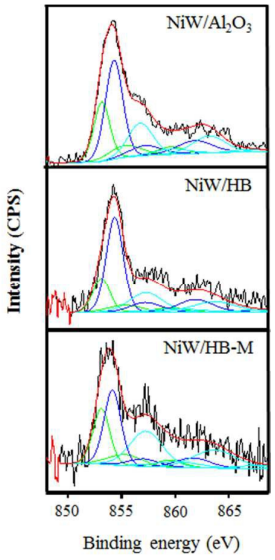

Figure 5. Emission region of Ni2p XPS spectra of various catalysts sulfided at 673 K with their fit decomposition curves: experimental (black), simulation (red), Ni_xS_y (green), NiWS (blue), Ni^{2+} (cyan).

The XPS spectra for Ni2p are presented in Figure 5. The fitting parameter for XPS decomposition in the energy emission region of Ni2p has been reported elsewhere[31]. Their decomposition evidenced three contributions: Nickel sulfides Ni_xS_y (Ni2p3/2: 852.6 eV, Ni2p1/2: 869.8 eV), NiWS (Ni2p3/2: 853.7 eV, Ni2p1/2: 870.9

eV) and an oxidic phase Ni^{2+} (Ni2p3/2: 856.4 eV, Ni2p1/2: 873.8 eV)[25, 27, 31, 32]. The proportions of NiO, Ni_xS_y and NiWS in the catalysts were calculated and listed in Table 4. The proportion of NiWS species is representative of the promotion degree of WS_2 slabs by the Nickel. A proportion of 44% NiWS was obtained in NiW/Al_2O_3, which was similar to that in the previous work[32]. Comparatively, the promotion degree of Ni was 52% and 33% in NiW/HB and NiW/HB-M, respectively.

Table 4. Percentage of various Ni species in catalysts after sulfidation

Samples	NiWS (%)	Ni_xS_y (%)	Ni^{2+} (%)
NiW/Al_2O_3	44	27	29
NiW/HB	52	20	28
NiW/HB-M	33	26	41

Representative TEM images of the sulfided catalysts are shown in Figure 6. All the samples exhibited the typical structure of the layered WS_2 phase, with an interplanar spacing of 0.65 nm, corresponding to the (002) planes of the WS_2 crystal[36]. No agglomeration could be observed. By the statistical analysis of the images, the distributions in slab length and stacking of the WS_2 slabs were obtained (Figure 7). On sulfided NiW/Al_2O_3, the WS_2 slab length was between 1 and 10 nm with an average length (L) of 4.8 nm and an average stacking number (N) of 1.2. The length of WS_2 slabs in NiW/HB was distributed between 1 to 13 nm. The calculated average L and N were 4.8 nm and 3.3, respectively. Additionally, the length of WS_2 slabs in NiW/HB-M was distributed in a narrower range of 1~7 nm with average values of 2.6 nm (L) and 2.6 (N). It has been reported in earlier literatures that the active phase over zeolite support would be larger and more stacked than that over alumina support[14,28,34], which was in agreement with our results. This can be explained by a weaker interaction developed on the zeolite support by the sulfided phase compared to alumina, well known for its dispersion ability[14].

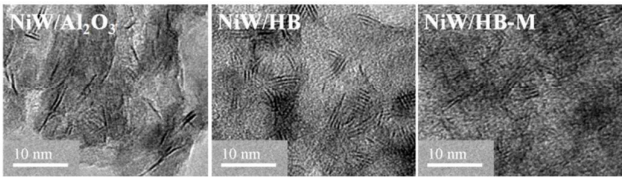

Figure 6. HRTEM images of sulfided NiW/Al_2O_3, NiW/HB and NiW/HB-M.

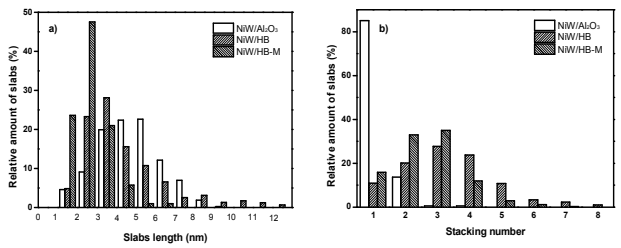

Figure 7. Distribution of the length (a) and stacking number (b) of the WS_2 slabs over various supports.

3.2. Catalytic evaluation

The catalytic performance of these catalysts was evaluated in the HDS of thiophene. The main HDS reaction pathway in this reaction was shown in Scheme 1. Only four products (1-butene, cis- and trans-2-butene, n-butane) can be detected over NiW/Al_2O_3. In comparison, some additional products (such as ethane, ethylene, propane and propene) were detected over NiW/HB and NiW/HB-M due to the strong acidity of the support. No dihydrothiophene, tetrahydrothiophene and 1,3-butadiene were detected because they can be quickly converted into butane and butenes. Moreover, a small amount of unidentified large molecules were detected over NiW/HB and NiW/HB-M, which might be attributed to the polymerization of olefins.

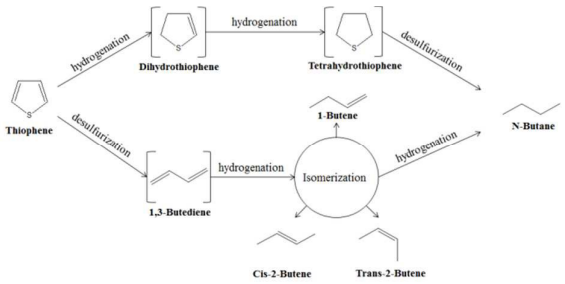

Scheme 1. Main reaction pathway for thiophene hydrodesulfurization.

The reaction rate of thiophene over various catalysts with time on stream was shown in Figure 8. The activities after 15 minutes and 3 hours of reaction over these catalysts are listed in Table 5. Here, we can consider the activity at a reaction time of 3 h as the steady-state because activity tended to be stable after this time. Obviously, no deactivation was observed over NiW/Al_2O_3 within a reaction time of 8 h with an activity around 177 $L.h^{-1}.mol^{-1}$ W. In comparison, NiW/HB displayed higher initial activity (385 $L.h^{-1}.mol^{-1}$ W) than NiW/Al_2O_3. However, rapid deactivation occurred and the catalytic activity was stabilized after a reaction time of 3 h. The steady-state activity of NiW/HB was 71 $L.h^{-1}.mol^{-1}$ W, which was much lower than that of NiW/Al_2O_3. Further, NiW/HB-M exhibited highest initial activity (473 $L.h^{-1}.mol^{-1}$ W) among these catalysts. Nevertheless, rapid deactivation was also observed over NiW/HB-M. After a reaction time of 3 h, the activity reached 195 $L.h^{-1}.mol^{-1}$ W.

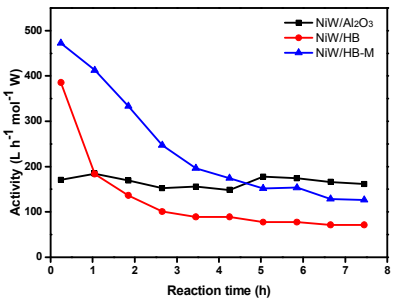

Figure 8. Catalytic activity of various catalysts with time-on-stream in HDS of thiophene.

Table 5. Initial and steady-state activity of various catalysts.

Catalysts	NiW/Al_2O_3	NiW/HB	NiW/HB-M
Initial activity (L h^{-1} mol^{-1} W)	177	385	473
Steady-state activity (L h^{-1} mol^{-1} W)	177	71	195

The steady-state selectivity of products over various catalysts was shown in Figure 9. Only n-butane, 1- and 2-butenes (C4 products) were observed over NiW/Al_2O_3. For NiW/HB, some cracking products (C2 2%, C3 12%) as well as polymerized products (others 14%) could be detected besides major C4 products (72%). Comparatively, NiW/HB-M exhibited higher cracking activity (C2 3%, C3 19%) than NiW/HB, which might be related to the larger number of accessible acid sites in HB-M as the number of acid sites located in mesopores/macropores could be less reduced than that in micropores during deactivation[21, 37].

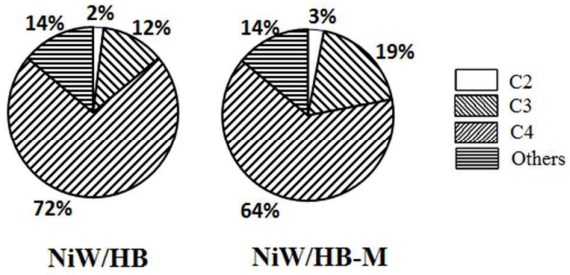

Figure 9. Product selectivity of NiW/HB and NiW/HB-M at steady-state in HDS of thiophene.

4. Discussions

4.1. Location of NiW active phase

In general, the promotion degree in TMS catalysts should have a good relationship with the sulfidation degree because the existence of more species like $W(Mo)S_2$ can result in higher possibility of formation for the species like NiW(Mo)S. In this work, although NiW/HB-M exhibited higher sulfidation degree (58%) than NiW/Al_2O_3 (30%), the promotion degree in NiW/HB-M (33%) was lower than that in NiW/Al_2O_3 (44%). Similarly, the sulfidation degree in NiW/HB (73%) was twice more than that in NiW/Al_2O_3 (30%) while the promotion degree (52%) in NiW/HB was only slightly higher than that (44%) in NiW/Al_2O_3. This means that Ni species might not efficiently promote the sulfided W species in HB and HB-M.

To explain the above results, an imaginative diagram about the distribution of active phase in micropores and mesopores/macropores of zeolite Beta was proposed (Scheme 2). As shown, Ni species might be located in both micropores and mesopores/macropores of zeolite Beta, whereas W species could be only located in mesopores/macropores. Such supposition was mainly based on the consideration of preparation process for the introduction of the active phase. In this work, the precursors of active phase were nickel nitrate hexahydrate and ammonium metatungstate. During the impregnation, Ni^{2+} from the precursor of Ni species can enter the pores of zeolite Beta, including micropores, due to its small cation size. However, it will be more difficult for $H_2W_{12}O_{40}^{6-}$ from the precursor of W species to enter the micropores because the size of the anion is relatively large. Ni species might thus be located in both micropores and mesopores/macropores of zeolite Beta and W species only in mesopores/macropores. This means that only Ni species located in mesopores can play a promotion role on WS_2. This hypothesis can explain why NiW/HM and NiW/HM-M with high sulfidation degree did not accordingly display high promotion degree.

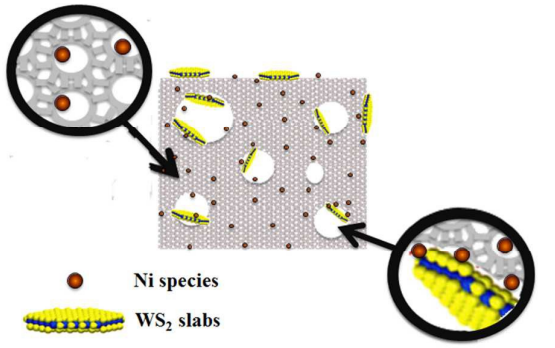

Scheme 2. Proposed imaginative diagram about location of active phase in hierarchical Beta.

4.2. Deactivation of hierarchical Beta supported catalyst

As shown in Figure 8, NiW/HB-M and NiW/HB exhibited largely higher initial activity than NiW/Al_2O_3. The higher initial activity of NiW/HB than NiW/Al_2O_3 might be partly attributed to its higher sulfidation/promotion degree. However, NiW/HB-M showed higher initial activity than NiW/HB, which was different to the order of their sulfidation/promotion degrees. It could be assumed that due to very fast deactivation at the beginning of the reaction observed in Figure 8 for zeolite based catalysts, the initial activity value is difficult to measure with a good accuracy. On the other hand, the additional mesopores in zeolite support could improve the performance of zeolite based catalysts as already reported[38].

Activity after 3 hours of NiW/HB and NiW/HB-M is much lower than their corresponding initial activity and after 6 hours it becomes

below that of NiW/Al_2O_3. It is well known that zeolite deactivated easily in many acid-catalytic reactions due to coke formation[20-22, 37, 39]. Such initial deactivation caused by rapid coke formation has also been reported when zeolite was used as support of Ni hydrotreating catalyst[40]. It was indicated that the amount of coke in zeolite supported catalyst quickly increased during the beginning of reaction, and then tended to be stable. In this work, the initial deactivation over NiW/HB and NiW/HB-M in HDS reaction of thiophene could be possibly attributed to coke formation due to the strong acidity from zeolite Beta.

In this work the introduction of additional mesopores/macropores in zeolite Beta did not inhibit the deactivation tendency even if in literature data, introduction of hierarchical pores in zeolite is reported to remarkably retard the deactivation caused by coke formation[20-22,37]. Indeed coke formation is known to preferably occur inside the micropores that can block or cover active sites[41]. In this case external active sites outside micropores are available to perform the catalytic function even when active sites inside micropores are deactivated[21]. The distribution of active sites in both micropores and mesopores/macropores in hierarchical zeolite could then explain the anti-deactivation ability. In our case, NiW/HB-M did not exhibit better anti-deactivation ability than NiW/HB that can be due to the single distribution of active species in mesopores/macropores as shown in Scheme 2.

4.3. Improvement of the anti-deactivation ability of hierarchical Beta supported catalyst

Considering that this deactivation might be caused by the coke formation, it was attempted to mix NiW/HB-M with NiW/Al_2O_3 in different proportions to inhibit deactivation as the additional alumina could trap coke precursors on the alumina surface[42] and decrease the acidity of the catalyst. The comparison of the acidity of different supports obtained by NH_3-TPD is listed in Table 6. Obviously, the support Al_2O_3 support possesses the least number of acid sites and the weakest acidity.

Table 6. Acidity of different supports measured by NH_3-TPD.

Samples	Desorption temperature (°C)		Number of acid sites (μmol/g)
Al_2O_3	249	-	204
HB	280	450	1170
HB-M	260	440	920
NaB	290	-	910
NaB-M	280	-	600

The catalytic activities of mixed catalysts in the HDS of thiophene are presented in Figure 10. Obviously, the addition of NiW/Al_2O_3 into NiW/HB-M greatly inhibited the deactivation of the catalysts. The deactivation of NiW/HB-M was remarkably inhibited when the content of NiW/Al_2O_3 was increased to 80 wt% (NiW/20HB-M). The steady-state activity of NiW/20HB-M (276 $L.h^{-1}.mol^{-1}$ W) was about 1.5 times as that of NiW/HB-M (195 $L.h^{-1}.mol^{-1}$ W) and NiW/Al_2O_3 (177 $L.h^{-1}.mol^{-1}$ W). The same method was also used to prepare the mixed catalyts of NiW/HB and NiW/Al_2O_3. The result indicated that deactivation can be also inhibited by this strategy. However, the steady-state activity (212 L h^{-1} mol^{-1} W) of NiW/20HB with the same content of NiW/Al_2O_3 was still lower than that of NiW/20HB-M.

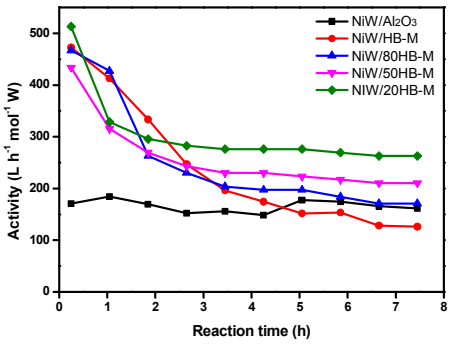

Figure 10. Catalytic activity of mixed catalysts with time-on-stream in HDS of thiophene

Another strategy to inhibit the deactivation was to use Na^+-exchanged Betas as support of NiW catalysts, by reducing the acidity of the support. It can be seen from the results of NH_3-TPD that H-form Beta possessed both strong and weak acid sites. After Na^+ ion-exchange, the desorption peak corresponding to the strong acid sites in H-form Beta disappeared (Fig. 11), suggesting the ion exchange process is efficient for decreasing the acidity of H-Beta.

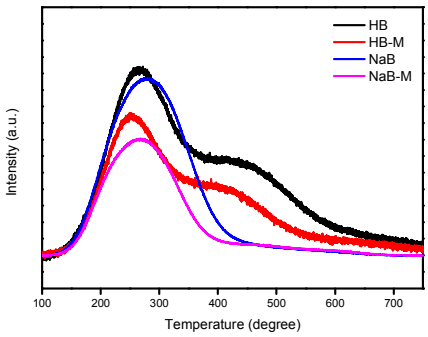

Figure 11. NH_3-TPD profiles for various samples.

Their catalytic activities were shown in Figure 12 and show that deactivation can be restrain by using Na^+ exchanged zeolites. NiW/NaB-M exhibited a steady-state activity 330 $L.h^{-1}.mol^{-1}$ W that can be compared to that of NiW/HB-M equal to 195 $L.h^{-1}.mol^{-1}$ W.

Also, a similar effect was observed over NiW/NaB presenting an improved steady-state activity reaching 190 $L.h^{-1}.mol^{-1}$ W. These results clearly indicate that deactivation was greatly inhibited by this strategy and thus the catalytic performance of both NiW/HB and NiW/HB-M was remarkably improved. However, some authors reported that the sodium ion exchange on zeolite could negatively influence the crystallinity of zeolite, which might affect the hydrothermal stability of zeolite. The alumina-silicous skeleton and framework might be easily damaged in the process of regeneration[43].

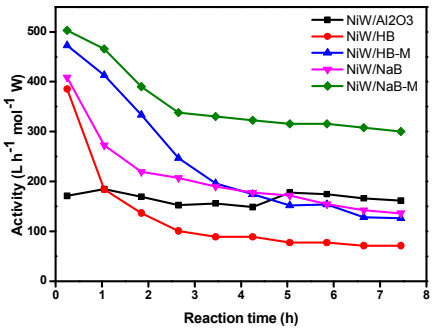

Figure 12. Catalytic activity of various catalysts with time-on-stream in HDS of thiophene.

This enhancement could also be observed with other zeolite type such as mordenite zeolite supported TMS catalysts (SI). The further characterizations to clarify the deactivation effect on Na^+ exchanged Beta supported NiW catalysts is underway.

Conclusions

NiW catalysts supported on γ-Al_2O_3 (NiW/Al_2O_3), commercial Beta (NiW/HB) and hierarchical Beta (NiW/HB-M) were prepared and their catalytic performance was evaluated by HDS of thiophene. NiW/HB and NiW/HB-M exhibited higher initial catalytic activity than NiW/Al_2O_3. However, important deactivation occurred over NiW/HB and NiW/HB-M showing that the introduction of additional mesopores/macropores in HB-M support could not prevent the deactivation tendency. This could be explained by the location of active phase (WS_2 and NiWS species) supposed to be located outside micropores.

Additionally, two methods have been attempted to improve the catalytic performance of NiW/HB-M in HDS of thiophene by inhibiting the deactivation of catalyst. One method is the mechanical mixing of NiW/HB-M with NiW/Al_2O_3. The other one is the use of Na^+-exchanged zeolite as support of NiW catalyst. Both methods are very efficient and lead to steady-state activities 1.5 times and twice higher respectively than that of NiW/Al_2O_3, reference catalyst.

Acknowledgements

Martine Trentesaux is acknowledged for catalysts characterization by XPS. Olivier Gardoll is acknowledged for NH_3-TPD experiments. Laurent d'Apolito is acknowledged for the homemade IR glass cell design and realization. The TEM facility in Lille (France) is supported by the Conseil Regional du Nord-Pas de Calais, and the European Regional Development Fund (ERDF). The authors acknowledge the financial support from the Fundamental Research Funds for the Central Universities (Grant No. HIT. NSRIF. 2015046), the Scientific Research Starting Funding from Harbin Institute of Technology, the Scientific Research Foundation for the Returned Overseas Chinese Scholars, State Education Ministry, and the Program Caiyuanpei (project N°30323NF) between China (CSC)–France (Campus-France).

Notes and references

1 A. Stanislaus, A. Marafi, M.S. Rana, *Catal. Today*, 2010 **153**, 1.
2 H. Topsoe, B.S. Clausen, F.E. Massoth, in: J.R. Anderson, M. Boudart (Eds.), *Catalysis – Science and Technology. Hydrotreating Catalysis*, 1996, **11**, 310.
3 P.A. Nikulshin, V.A. Salnikov, A.V. Mozhaev, P.P. Minaev, V.M. Kogan, A.A. Pimerzin, *J. Catal.*, 2014, **309**, 386.
4 J. Marques, D. Guillaume, I. Merdrignac, D. Espinat, S. Brunet, *Appl. Catal. B*, 2011, **101**, 727.
5 B. Pawelec, J.L.G. Fierro, A. Montesinos, T.A. Zepeda, *Appl. Catal. B*, 2008, **80**, 1.
6 V. La Parola, M.L. Testa, A.M. Venezia, *Appl. Catal. B*, 2012, **119-120**, 248.
7 S.A. Giraldo, A. Centeno, *Catal. Today*, 2008, **133-135**, 255.
8 A.M. Venezia, R. Murania, V. La Parola, B. Pawelec, J.L.G. Fierro, *Appl. Catal. A*, 2010, **383**, 211.
9 W. Chen, F. Mauge, J. van Gestel, H. Nie, D. Li, X. Long, *J. Catal.*, 2013, **304**, 47.
10 Y. Wang, B. Wang, A. Rives, Y. Sun, *Energy and Environment Focus*, 2014, **3**, 1.
11 D. Zhang, A. Duan, Z. Zhao, X. Wang, G. Jiang, J. Liu. C. Wang, M. Jin, *Catal. Today*, 2011, **175**, 477.
12 D. Solis, A.L. Agudo, J. Ramirez, T. Klimova, *Catal. Today*, 2006, **116**, 469.
13 Q. Huo, T. Dou, Z. Zhao, H. Pan, *Appl. Catal. A*, 2010, **381**, 101.
14 Y. Fan, H. Xiao, G. Shi, H. Liu, Y. Qian, T. Wang, G. Gong, X. Bao, *J. Catal.,* 2011, **279**, 27.
15 F. Bataille, J.L. Lemberton, G. Perot, P. Leyrit, T. Cseri, N. Marchal, S. Kasztelan. *Appl. Catal. A,* 2001, **220**, 191.
16 D. Solis, T. Klimova, R. Cuevas, J. Ramirez, A. Lopez-Agudo, *Catal. Today*, 2004, **98**, 201.
17 Q. Huo, Y. Gong, T. Dou, Z. Zhao, H. Pan, F. Deng, *Energy & Fuels*, 2010, **24**, 3764.
18 K.T. Hojholt, P.N.R. Vennestrom, R. Tiruvalam, P. Beato, *Chem. Comm.*, 2011, **47**, 12864.
19 T. Tang, L. Zhang, W. Fu, Y. Ma, J. Xu, J. Jiang, G. Fang, F.-S. Xiao, *J. Am. Chem. Soc.*, 2013, **135**, 11437.
20 R. Srivastava, M. Choi, R. Ryoo, *Chem. Commun.*, 2006, **43**, 4489.
21 J.-C. Kim, K. Cho, R. Ryoo, *Appl. Catal. A,* 2014, **470**, 420.
22 Y. Liu, N. Zhao, H. Xian, Q. Cheng, Y. Tan, N. Tsubaki, X. Li, *ACS Appl. Mater. Interfaces*, 2015, **7**, 8398.
23 Y. Wang, Y. Sun, C. Lancelot, C. Lamonier, J. Morin, B. Revel, L. Delevoye, A. Rives, *Micropor. Mesopor. Mater.*, 2015, **206**, 42.
24 K. Ben Tayeb, C. Lamonier, C. Lancelot, M. Fournier, E. Payen, A. Bonduelle, F. Bertoncini, *Catal. Today*, 2010, **150**, 207.

25 K. Ben Tayeb, C. Lamonier, M. Fournier, E. Payen, F. Bertoncini, A. Bonduelle, *Am. Chem. Soc. Div. Fuel chem.*, 2008, **53**, 9.
26 C. Martin, C. Lamonier, M. Fournier, O. Mentre, V. Harle, D. Guillaume, E. Payen, *Chem. Mater.*, 2005, **17**, 4438.
27 K. Ben Tayeb, C. Lamonier, C. Lancelot, M. Fournier, A. Bonduelle, F. Bertoncini, *Appl. Catal. B*, 2012, **126**, 55.
28 L. Ding, Y. Zheng, Z. Zhang, Z. Ring, J. Chen, *J. Catal.*, 2006, **241**, 435.
29 L. Ding, Y. Zheng, Z. Zhang, Z. Ring, J. Chen, *Appl. Catal. A*, 2007, **319**, 25-37.
30 R. Tian, B. Shen, F. Wang, C. Lu, C. Xu, *Energy & Fuels*, 2009, **23**, 55.
31 J.N. Diaz de Leon, M. Picquart, L. Massin, M. Vrinat, J.A. de los Reyes, *J. Mole. Catal. A*, 2012, **363-364**, 311.
32 H.R. Reinhoudt, E. Crezee, A.D. van Langeveld, P.J. Kooyman, J.A.R. van Veen, J.A. Mouljin, *J. Catal.*, 2000, **196**, 315.
33 G. Wan, A. Duan, Y. Zhang, Z. Zhao, G. Jiang, D. Zhang, Z. Gao, J. Liu, K.H. Chung, *Energy & Fuels*, 2009, **23**, 3846.
34 L. Ding, Y. Zheng, H. Yang, R. Parviz, *Appl. Catal. A,* 2009, **353**, 17.
35 Y.V. Joshi, P. Ghosh, M. Daage, W.N. Delgass, *J. Catal.*, 2008, **257**, 71.
36 B.S. Zhang, Y.J. Yi, W. Zhang, C.H. Liang, D.S. Su, *Mater. Charact.*, 2011, **62**, 684
37 H. Yang, Z. Liu, H. Gao, Z. Xie, *Appl. Catal. A,* 2010, **379**, 166.
38 Y. Wang, J. Wu, S. Wang, *RSC Adv.*, 2013, **3**, 12635.
39 M. Guidotti, C. Canaff, J.-M. Coustard, P. Magnoux, M. Guisnet, *J. Catal.,* 2005, **230**, 375.
40 J. Aguado, D.P. Serrano, J.M. Escola, L. Briones, *Fuel*, 2013, **109**, 679.
41 M.L. Occelli, J.P. Olivier, A. Auroux, *J. Catal*., 2002, **209**, 385.
42 J.S.J. Hargreaves, A.L. Munnoch, *Catal. Sci. Technol.*, 2013, **3**, 1165.
43 L.-E. Sandoval-Diaz, L.-A. Palomeque-Forero, C.A. Trujillo, *Appl. Catal. A*, 2011, **393**, 171.